

## Article

# Response of the Thick and Thin Debris-Covered Glaciers between 1971 and 2019 in Ladakh Himalaya, India—A Case Study from Pensilungpa and Durung-Drung Glaciers

Manish Mehta <sup>1,\*</sup> , Vinit Kumar <sup>1,\*</sup> , Pankaj Kunmar <sup>1,2</sup> and Kalachand Sain <sup>1</sup><sup>1</sup> Wadia Institute of Himalayan Geology, Dehradun 248001, India<sup>2</sup> Department of Geology, Hemvati Nandan Bahuguna Garhwal University, Srinagar 246174, India

\* Correspondence: msmehta75@gmail.com (M.M.); vinitkumark17@gmail.com (V.K.)

**Abstract:** This paper aims to broadly understand the response of glaciers to thick and thin debris cover from one of the less explored regions (Zaskar) of the Himalaya. The present study is based on ground-based measurements (from 2015 to 2019), satellite data (since 1971), and available topographic maps (at a 1:50,000 scale). The study includes snout retreat, changes in equilibrium line altitude (ELA), surface elevation, and modeled mass balance of thick and thin debris-covered Pensilungpa (Suru River basin) and Durung-Drung (Doda River basin) glaciers in the western Indian Himalaya, Ladakh, for the past five decades. The Durung-Drung Glacier (DDG) receded  $\sim -624 \pm 547$  m with an average rate of  $-12 \pm 11$  m a<sup>-1</sup> between 1971 and 2019. The frontal part of the DDG is broad ( $\sim 2$  km wide), which shows wide discrepancies in its retreat. Compared to DDG, the small and narrow snout of the Pensilungpa Glacier (PG) retreated  $-270.5 \pm 27.5$  m (1971 to 2019), with an average rate of  $-5.6 \pm 0.57$  m a<sup>-1</sup>. Similarly, the four years (2015–2019) of field observations suggest that the retreat rate of PG and DDG is  $-6.7 \pm 3$  and  $-18 \pm 15$  m a<sup>-1</sup>, and the rate of modeled glacier mass loss is  $-0.29 \pm 0.3$  and  $-0.3 \pm 0.3$  m w.e. a<sup>-1</sup>, respectively. Furthermore, the ELA of the DDG and PG between 1971 and 2019 increased by  $\sim 59 \pm 38$  and  $\sim 23 \pm 19$  m, respectively. The change in the longitudinal profile of the glaciers along the centerline between 2000 and 2017 shows the DDG and PG lost  $\sim 17$  and 15 m surface ice thickness. The change in debris cover plays a critical role in the glacier surface lowering, shrinkage, retreat, and mass balance. Hence, we quantitatively evaluated the influence of the debris cover on summer ablation and terminus recession on two different characteristic glaciers (DDG and PG) with its potential effect on the mass balance process (area-volume loss).

**Keywords:** Pensilungpa Glacier; Durung-Drung Glacier; snout retreat; equilibrium line altitude; Ladakh Himalaya



**Citation:** Mehta, M.; Kumar, V.; Kunmar, P.; Sain, K. Response of the Thick and Thin Debris-Covered Glaciers between 1971 and 2019 in Ladakh Himalaya, India—A Case Study from Pensilungpa and Durung-Drung Glaciers. *Sustainability* **2023**, *15*, 4267. <https://doi.org/10.3390/su15054267>

Academic Editors: David Pulido-Velázquez, Antonio Juan Collados-Lara and Aynur Sensoy

Received: 23 November 2022

Revised: 16 February 2023

Accepted: 24 February 2023

Published: 27 February 2023



**Copyright:** © 2023 by the authors. Licensee MDPI, Basel, Switzerland. This article is an open access article distributed under the terms and conditions of the Creative Commons Attribution (CC BY) license (<https://creativecommons.org/licenses/by/4.0/>).

## 1. Introduction

It is widely recognized that glaciers are highly sensitive to climatic change, and a lot of research has been focused on the response to increased global temperature (since 1950 onwards) and on evaluating future changes under the present climate change scenarios [1]. Changes in glacier mass balance and its components are the most reliable indicators of climatic change [2]. These are determined by winter accumulation (snowfall) and summer ablation (melting), which are, in turn, driven by anomalies in global and regional atmospheric circulation, as well as changes in local weather patterns and specific glacier characteristics (e.g., altitude, aspect, and supraglacial debris) [3–5]. The Himalaya contains thousands of glaciers of widely varying properties, which are spread over nearly 37,000 km<sup>2</sup> with an east-west range of >2000 km [6]. One of the significant characteristics of the Himalayan glaciers is that the glaciers are mainly debris-covered (70–80%) and have been receding since the end of the Little Ice Age [5,7–13]. The supraglacial debris on the surface of glaciers is commonly found to have significant control over the rate of ice ablation

and recession [4,9,14–20]. It has been observed that the thickness of supraglacial debris significantly alters the glacier response to climate forcing [11,21,22]. Using remote sensing and field-based data in different parts of the Himalaya, several studies, such as mapping debris cover and its correlation with glacier melting and recession, have been carried out [10,11,16,19,21–24]. As a consequence of the complex climate system, glacial geometry, glacier surface properties, and geology, the recession rates of the glaciers are variable [21]. The studies suggest that most of the Himalayan glaciers are retreating between 5 and 20 m a<sup>-1</sup> with the negative mass balance varying between 0.2 to 1.2 m w. e. a<sup>-1</sup> and ELA fluctuations from 4900 and 5300 m asl [5,10]. Glaciers are key markers of understanding climate change, so monitoring of glaciers in terms of estimating the overall changes of mass, volume, area, and length over space and time is essential. Despite the importance of the Himalayan glaciation, the knowledge of the glacial dynamics and forcing factors is scanty [10,25]. Recent studies of Himalayan glaciers indicate wide variability in terminus retreat rate and mass balance in different sectors of the mountain range, primarily linked to the topography and climate of the region [10,26–28]. However, variable retreat rates of glacier termini and inadequate supporting field data (e.g., mass balance, ice thickness, velocity, etc.) of the Himalayan glaciers make it challenging to develop a coherent picture of climate change impact.

In this study, we selected two glaciers with different characteristics, i.e., the Pensilungpa Glacier (PG) in Suru River and Durung-Drung Glacier (DDG) in Doda River basins, for a comparative study of glacier fluctuations between 1971 and 2019. The PG is characterized by a thick debris cover, while the DDG has a thin debris cover. The purpose of this study is to (i) measure the frontal retreat and area loss by the glaciers, (ii) reconstruct the present and past ELA followed by validation with field-based ELA, and (iii) estimate the centerline thickness lost by the glacier and mass balance.

### 1.1. Study Site

The DDG (30°46′11.93″ N–76°18′45.14″ E) and PG (33°49′5.37″ N–76°17′06.44″ E) are located in the SE and SW direction of Pensi-La pass (4454 m asl), respectively (Figure 1). DDG is the source of the Doda River, which originates from 4121 m asl and flows in the SE direction. The Doda River is the largest tributary of the Zaskar River (a tributary of the Indus River) and receives meltwater from 697 glaciers covering ~1080 km<sup>2</sup> glacierized area [29]. The NE-facing, 23 km long DDG is the largest glacier in the valley occupying an area of ~72 km<sup>2</sup>. The glacier is almost clean, only 5.5% of the ablation area is covered by thin and scattered debris, and the average glacier slope is ~6°. The DDG is a compound valley-type glacier. The accumulation zone is broad with a gentle slope, formed by >6 cirques (Figure 1). The ablation zone of the glacier is narrower than the accumulation zone. It is bounded by well-preserved series of lateral and recessional moraines, indicating the glacier's dynamic behavior and past extent.

Similarly, the Suru River (a tributary of the Indus River) originates from the PG at an altitude of 4670 m asl. The Suru Basin is supported by 252 glaciers, covering an area of 481 km<sup>2</sup>, 11% of the total area [20]. The entire length of PG is ~8 km, covering an area of ~16 km<sup>2</sup> (including tributary glaciers), and ~17% of its overall glaciated area is covered with debris of varying thickness, which constitutes 30% of the ablation area. The PG is north-flowing and originates from the valley's southwest slope with an average gradient of 8°, and terminates at an elevation of ~4670 m asl. Several longitudinal and transverse crevasses, small supraglacial ponds, and ice cliffs are present on the PG's surface (in the ablation zone).

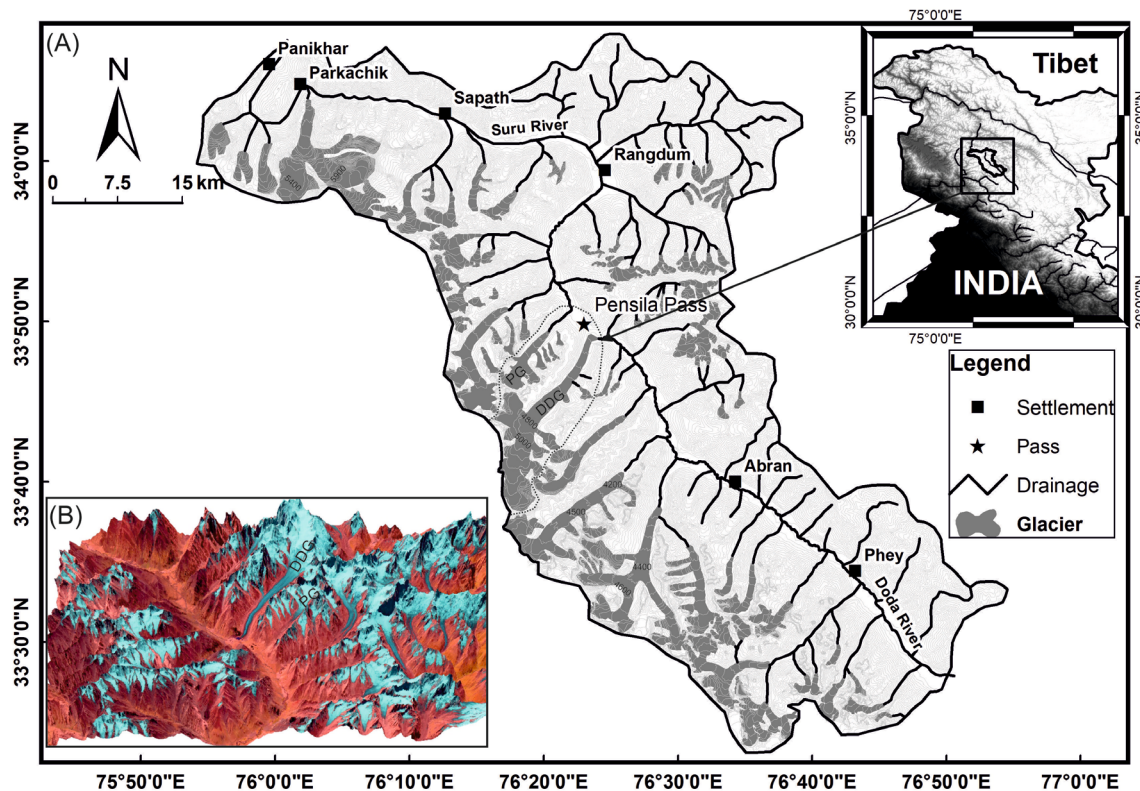


**Figure 1.** Location and contour map of the study area, (A) showing glacial distribution in Suru and Doda basins and black dash line indicates the boundary of Pensilungpa Glacier (PG) and Durung-Drung Glacier (DDG) catchments. The inset India map shows the location of the study area. (B) Digital Elevation Model (DEM) of DDG and PG showing the glaciers and snow cover in the study area.

The distribution of debris cover over the glacier follows a common pattern: the debris thickness decreases with increasing distance from the snout and elevation. Field observations (2015–2019) suggested that in the lower ablation zone (at the snout ~4700 m asl), the PG has a thick debris cover, and the thickness ranges between 15 and 40 cm. However, the upper ablation zone of PG (>4800 m asl) is thin debris-covered, and the debris thickness varies from 2 to 7 cm. In comparison, the ablation zone of DDG is partially debris-covered. The peculiar feature of DDG is that the glacier's center flowline is almost clean, and the left and right margins of the glacier are debris-covered.

### 1.2. Climate of the Study Area

The climate of the study area is controlled by the Indian Summer Monsoon and westerly circulations [5,30], and is temperate during summer and extremely dry and cold in winter. Due to the absence of instrumental data in the study area, we have used the Climate Research Unit Time Series (CRU-TS 4.03) data [5,31] to understand the climatic conditions. Here we present the temperature and precipitation of the interpolated gridded data (30.755 N and 79.250 E) derived from CRU-TS 4 for 117 years (1901–2018) for peak months of accumulation period (January, February, November, and December) and melting period (June–September). The result shows that the February, November, and December temperature gradually increases, and the precipitation in January and December decreases. However, the temperature of June, July, and August shows decreasing trend, while the September temperature shows an increasing trend.

Similarly, the precipitation in June shows an increase, whereas no changes have been observed for the rest of the summer months. The increased temperature of early winter and late summer demonstrated the prolonging of the summer period and the shortening

of winters. This increase in temperature (shift from solid to liquid precipitation) has been identified as one of the major factors responsible for the decrease in snowfall and enhanced melting of the glaciers over the Indian Himalayan region [5,10,20]. The mean monthly minimum temperature ( $-10\text{ }^{\circ}\text{C}$ ) was observed in January, and the average minimum monthly precipitation (11 mm) occurred in November. The maximum monthly mean temperature ( $18\text{ }^{\circ}\text{C}$ ) and average precipitation (71 mm) were recorded in July. Overall, the long-term (1901–2018) climate data shows an increased winter temperature trend and a decrease in winter precipitation after 2000 (Figure 2).

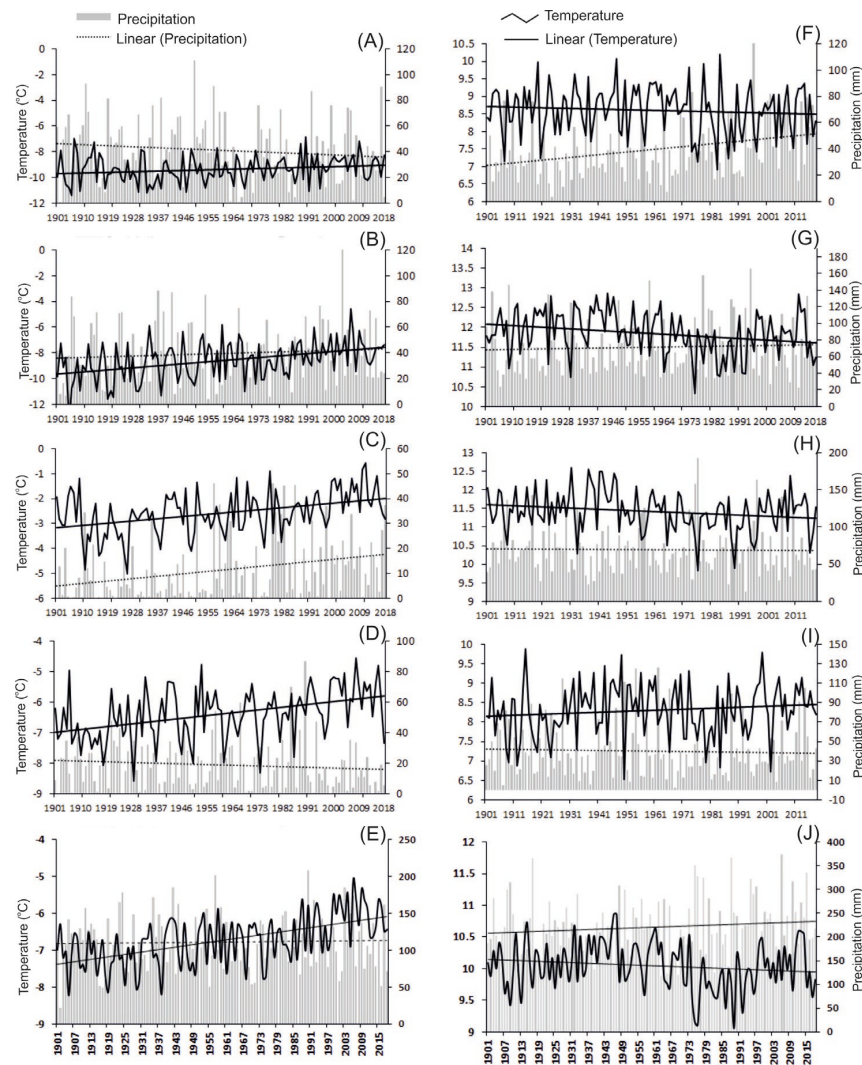


**Figure 2.** Annual and seasonal variability in the climatic conditions of the study area derived from CRU-TS 4.03 data (30.755 N and 79.250 E) for the period 1901–2018 (Modified after Mehta et al. [5]). The data are taken from the peak months of accumulation period (January (A), February (B), November (C), and December (D)) and melting period (June (F), July (G), August (H), and September (I)). (E,J) showing the winter and summer variability, respectively. The result shows that the temperature of February (B), November (C), and December (D) is gradually increasing and the precipitation of January (A) and December (D) is decreasing. However, the temperature of June (F), July (G), and August (H) shows decreasing trend, while the September (I) temperature shows an increasing trend. Similarly, the precipitation of June shows an increase, whereas for the rest of the summer month no change has been observed. Overall, the long-term (1901–2018) climate data show an increased winter temperature trend and a decrease in winter precipitation after 2000.

## 2. Datasets and Methods

In this study, the snout retreat, changes in the ELA, surface elevation, and modeled mass balance of the thick and thin debris-covered Pensilungpa and Durung-Drung glaciers, western Himalaya, Ladakh, India, are estimated using multiple sources (satellite images and field observations) (Table 1).

**Table 1.** Data used for monitoring of glaciers in this study.

Sl. No.	Satellite Sensor	Date of Acquisition	Remarks on Quality	Spatial Resolution (m)	Scene/Product ID	Purpose	Source
1.	Corona KH-4B	28-09-1971	Cloud-free	5	DS1115-2282DA056/DS1115-2282DA057	Delineation of glacier boundary (DGB)	USGS
2.	Hexagon KH-9	06-10-1977	Partially cloud covered	7	DZB1213-500234L001001	DGB	USGS
3.	Landsat TM	27-08-1994	Partially cloud covered	30	LT51480361994239ISP00	DGB	USGS
4.	Landsat ETM+	04-09-2002	Cloud free	30	LE71480362000248SGS00	DGB	USGS
5.	Sentinel MSI	20-09-2017 & 15-09-2019	Cloud free	10	S2A_MSIL1C_201709-20T053641_N0205_R005_T43SET_20170920T053854_LC81480362019228LGN00	DGB	USGS
6.	Field data; GPS, DGPS measurements, stake measurements, and photographs	2015 to 2019	NA	Point data	NA	NA	Ground based

The satellite images were acquired from the US Geological Survey (USGS, website) with minimal cloud cover. We used medium-resolution declassified Corona KH-4B (spatial resolution of 5 m), Hexagon-KH-9 (7 m), low-resolution Landsat series sensors TM/ETM<sup>+</sup> (30 m), Sentinel multispectral instrument (MSI) scenes from 2017 and 2019 (10 m) and Advanced Spaceborne Thermal Emission and Reflection Radiometer (ASTER)-L1A imageries. The satellite images selected for this study are based on their suitability (minimum cloud (<10%) and seasonal snow cover) for the most accurate glacier mapping.

Primarily, the acquired satellite images were co-registered by the projective transformation method using the Landsat ETM<sup>+</sup> for 1999. However, the CORONA KH-4B and Hexagon KH-9 images were co-registered using a two-step approach (i) Projective transformation using 30 GCPs, and (ii) Spline adjustment of the subset image using the methodology used by many authors [20,32–34]. The identification of glaciers boundary (historic and recent) and mapping principles was followed by Shukla et al. [20,34] and Mehta et al. [5]. Glacier boundaries were mapped manually for different points in time (1971, 1977, 1994, 2000, 2015, 2016, 2017, 2018, 2019, and 2021). Furthermore, high-resolution imagery from Google Earth<sup>TM</sup> was also used for the accurate demarcation of the boundary of the glacier.

### 2.1. Field Survey

From 2015 onwards, the snout position, frontal area loss, and glaciological mass balance measurements are ongoing on the glaciers in the Suru and Doda River basins [5,28,34–36]. More than ten permanent reference points were fixed near the frontal area of the DDG and PG snout on stable ground (Figure 3).

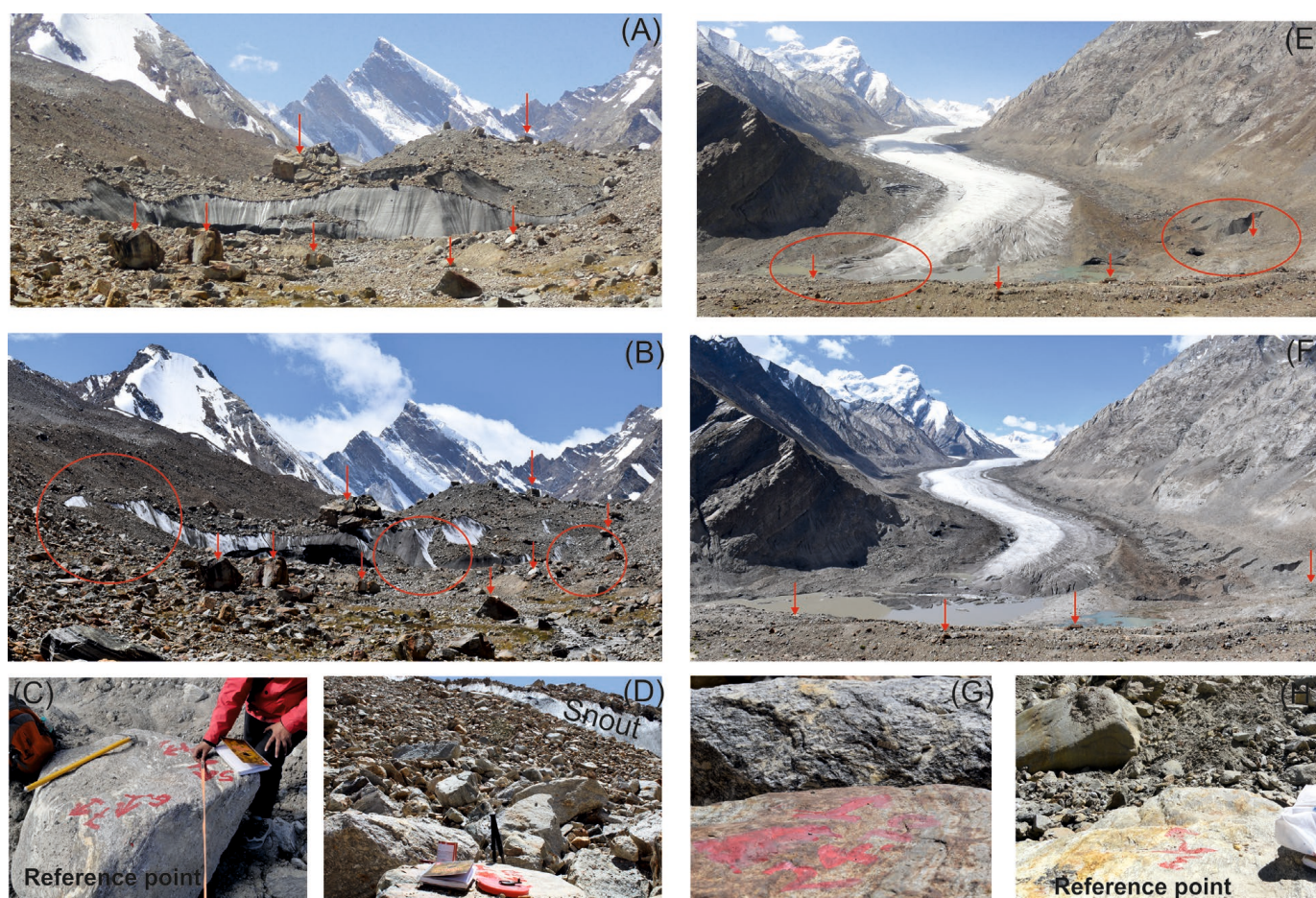


**Figure 3.** Field photographs showing the snout position of the glacier in 2015 and 2019 (Modified after Mehta et al. [5]), ((A,B), respectively) PG and ((E,F), respectively) DDG. Red circles on photograph (B,E) is indicating the area vacated by the glaciers and red arrows (in photographs (A,B) and (E,F)) are showing the reference points. (C,D,G,H) the close-up view of the reference points used for measuring the snout retreat with the help of chain tape survey.

The length from these reference points was then measured using a measuring scale up to the base of glacier ice from the left, right, and center of the snout. After that, the average length change was calculated based on the average recession from the glacier snout's left, right, and center parts for every studied year. The geographical position of each reference point was determined by Differential Global Positioning System (DGPS) and the real-time kinematic (RTK) points were taken with an accuracy of less than 0.1 m, with the base station set up at a distance of around 300 m from the glaciers snout. The obtained values were transferred on the map. We collected ten DGPS points, every year (2015 to 2019) at the margin of the snout of the DDG and PG and demarcated the frontal boundary of the glaciers. The glaciers front outlines of different years (e.g., 1971, 1977, 1994, 2000, and 2019) were plotted on the map to quantify the cumulative glacier frontal changes (Figure 4). Moreover, the field-based DGPS data of the glacier front were plotted on the map to calculate the frontal recession of the glacier between 2015 and 2019. In addition, we measured the recession from 2004 to 2019 using Google Earth imagery (Figure 4).

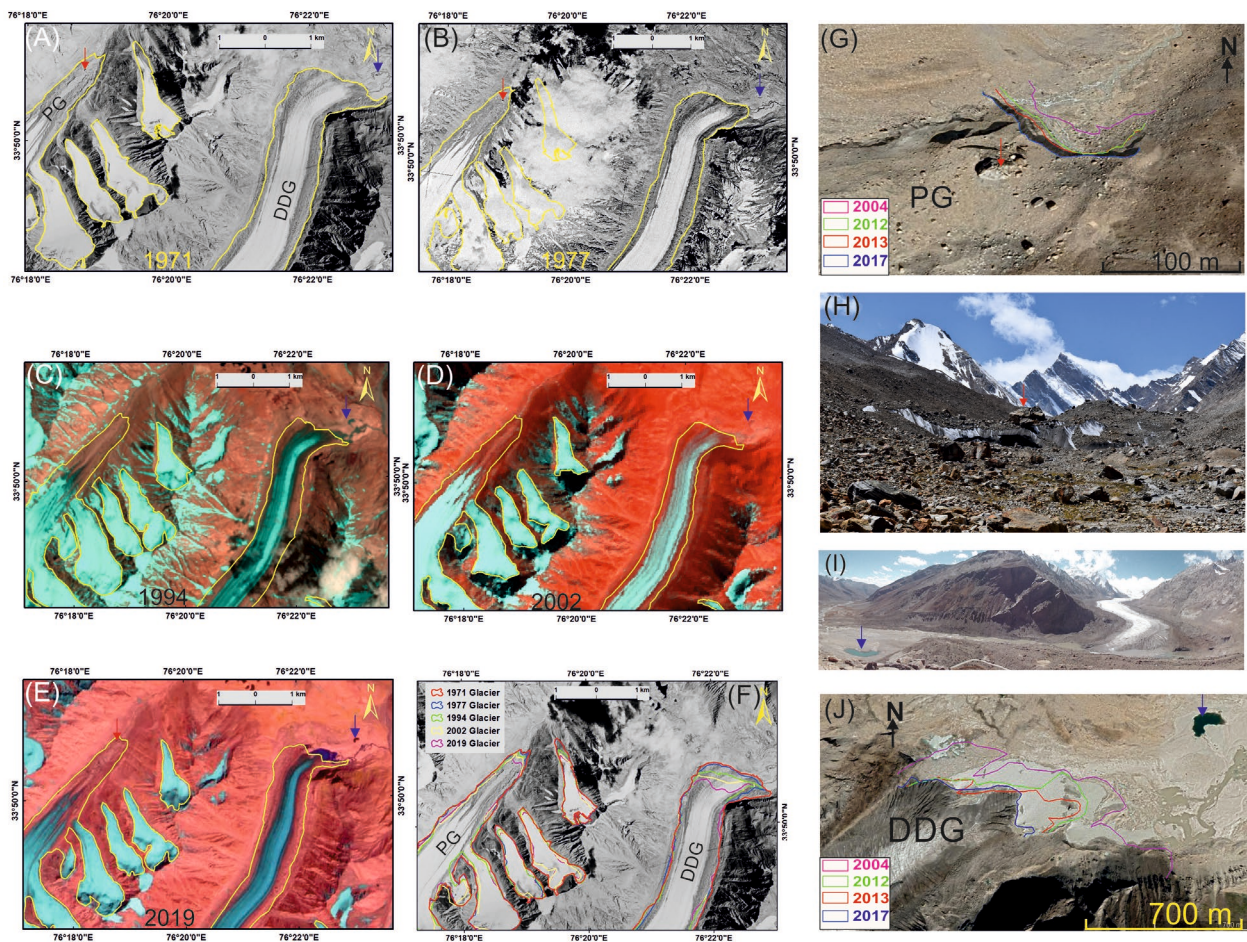


**Figure 4.** Temporal changes in the snout position of the PG and DDG during the period between 1971 and 2019 (Modified after Mehta et al. [5]). (A) The respective glacier boundaries for 28 September 1971 (Corona KH-4B), (B) 6 October 1977 (Hexagon KH-9), (C) 27 August 1994 (Landsat TM), (D) 4 September 2002 (Landsat ETM<sup>+</sup>), (E) 15 September 2019 (Sentinel Multispectral Imagery). (F) The glacier boundaries are dropped on the Corona KH-4B showing the glaciers recession between 1971 and 2019. (G) Snout retreat of PG measured using Google Earth Image during the periods between 2004 and 2017, (H) field photograph showing the snout of the PG and red arrow indicating reference point (big boulder). (I) Snout and proglacial kidney-shaped lake (blue arrow) of DDG, and (J) snout retreat of DDG during the periods between 2004 and 2017.

## 2.2. Estimation of Equilibrium Line Altitude (ELA)

The mass balance of the Himalayan glaciers is controlled by terrain, aspect, geographical position, and climatic condition of the area. The fluctuation of the ELA depends on the mass balance gradients of the glaciers. The modern ELA of the Himalayan glaciers ranges between 4400 to 5800 m asl [5,10,11,25,37,38]. The valley morphology, moraine location, and snout position help to understand the glacier's past and present ELA. To determine the valley morphology, moraine locations, and snout position of the glaciers we used satellite images, referenced topographic map (Survey of India 1:50,000) along with the field surveys (GPS/DGPS), and hypsometry was calculated from SRTM (90 m) data. The following hypsometrical methods are commonly used to reconstruct the ELA of the PG and DDG for 1971 and 2019 and validated with in situ measurements based on (i) Area Accumulation Ratio (AAR), (ii) Terminus to Headwall Altitude Ratio (THAR), (iii) Area Altitude Balance Ratio (AABR), and (iv) Maximum Elevation of Lateral Moraine (MELM) methods. To minimize the uncertainty in ELA estimation, an average of measurements using all these methods was used (Table 2) [39–50].

**Table 2.** Morphometric indices and their equation for estimate the ELAs of PG and DDG between 1966 and 2017.

Method	Equations	References	Remarks
Area Accumulation Ratio (AAR)	$AAR = \frac{Ac}{Ac+Ab}$	[39–42,50]	Here we used AARs of 0.45 (debris cover glaciers), 0.65 (less debris cover/clean glaciers) and 0.55 (all Himalayan glaciers) for estimate the present and past ELAs of the glaciers.
Terminus to Head Altitude Ratio (THAR)	$THAR = \frac{ELA-At}{Ah-At}$	[40,42–44,47]	The mass balance of north and north-western glaciers suggested that the THAR value of north-western Himalayan glaciers ranged between 0.5 and 0.6. Here we used these value for ELA Estimation.
Area Altitude Balance Ratio (AABR)	Spreadsheet	[40,42,47,48]	We used an Excel spreadsheet for the calculation the ELAs for the study glaciers using the method of AABR given by Osmaston (2005).
Maximum Elevation of Lateral Moraine (MELM)	-----	[41,42,45,49,50]	The Maximum altitude of Lateral moraines provide a secure means of determining the minimum altitude of former glacier ELAs.

### 2.3. Glacier Volume Estimation

The statistical regression relation of different approaches for estimating the ice volume of the glaciers was used in the present study. We used the following formula for ice volume calculation:

$$V = 0.04 S^{1.35} \quad (1)$$

V is glacier volume in km<sup>3</sup>, and S is glacier area in km<sup>2</sup>. This equation was derived by Liu et al. [51] based on thickness measurements by an ice-penetrating radar on 22 glaciers in the Tien Shan and Qilian Shan, western China.

$$V = cA^\gamma \quad (2)$$

V representing the glacier volume, A the glacier area, and c and  $\gamma$  are the two scaling parameters.

Here, we used three sets of scaling parameters, which have been applied by Cogley [52] and Frey et al. [53] for the Himalaya–Karakoram region. This equation is also used for all ICIMOD glacier inventories [54,55]. This equation was derived by Chen and Ohmura [56], who used measurements from 63 glaciers to determine the related scaling parameters. Bahr et al. [57] derived the parameters in a theoretical study and LIGG et al. [58] established a thickness–area relation based on ice-thickness measurements on 15 glaciers [59]. According to Cogley [52], the scaling parameters are given in Table 3.

**Table 3.** Scaling parameters for thickness estimation are taken from Cogley [52].

Factor c	Exponent $\beta$	Remark
0.1910	0.375	144 glaciers
0.2055	0.360	61 glaciers
0.8433	0.300	$a = -11.32$ m in expression, $H = a + cS^\beta$
0.2800	0.375	Western Chugach Mountains, southern Alaska
0.2100	0.350	Southern British Columbia, Canada

Haeberli and Hoelzle [60] presented an approach for estimating glacier volume based on the average surface slope and vertical glacier extent. The following formula is used to calculate the volume based on mean ice thickness along the central flowline:

$$hf = \frac{\tau}{f\rho g \sin(\sigma)} \quad (3)$$

where  $\tau$  is the average basal shear stress along the central flow line,  $f$  is a shape factor,  $g$  is the gravitational acceleration ( $9.81 \text{ m/s}^2$ ),  $\rho$  is the density of ice ( $917 \text{ kg m}^3$ ), and  $\alpha$  is the mean surface slope along the central flowline.  $f$  is chosen constant as 0.8, considered the typical value for valley glaciers [2]. The estimation of the mean ice-thickness of the entire glacier ( $hF$ ) came out through the extrapolation from the mean ice-thickness along the central flowline ( $hf$ ), following the assumptions of a semi-elliptic cross-sectional geometry and a non-branched glacier, a multiplication with  $(\pi/4)$  is added to Equation (3):

$$hF = hf \left( \frac{\pi}{4} \right) \quad (4)$$

#### 2.4. Glacier Mass Balance and Surface Elevation Change

Several researchers have used AAR and ELA methods to estimate the glacier mass balance in different parts of the world [11,61–66]. These studies have suggested that the specific mass balance can be calculated from the ELA and AAR [11,61,62,66–68]. Kulkarni et al. [67] developed a regression equation between AAR and specific mass balance to estimate the mass balance in the Indian Himalaya (Equation (5)). This regression equation between AAR and specific mass balance was derived from the in-situ measurements of two glaciers (Shaune Garang and Gor Garang) in the western Himalaya. This study suggested 0.5 AAR for zero mass balance. The relationship is

$$Y = 2.4301 \times X - 1.20187 \quad (5)$$

where  $Y$  = mass balance of the glacier ( $\text{m w.e.a}^{-1}$ ) and  $X$  is the glacier's Area Accumulation Ratio (AAR). The AAR-based empirical relationship was derived by Pratap et al. [11] from the mass balance data of 11 glaciers of the Indian Himalayas from NE to NW. They suggested that the steady-state AAR of the glaciers is  $\sim 0.55$  and the balanced budget ELA of the glaciers is  $\sim 5000 \text{ m asl}$ . Hence, the relationship between specific mass balance (in  $\text{m w.e.}$ ) and AAR takes the form (Figure 5A).

$$Y = 1.9433 \times X - 1.3149 \quad (6)$$

where  $Y$  = Specific mass balance ( $\text{m w. e. a}^{-1}$ ) and  $X$  is the AAR.

Similarly, we developed the empirical relationship between ELA and specific mass balance derived from the in situ measurements of the 11 glaciers in the Indian Himalayas to estimate the glacier mass balance. The empirical relationship is (Figure 5B)

$$Y = -0.0011 \times Z + 5.0055 \quad (7)$$

where  $Y$  = Specific mass balance ( $\text{m w.e.a}^{-1}$ ) and  $Z$  is the ELA of the glacier.

This study uses these three empirical equations for specific mass balance estimation of the PG and DDG.

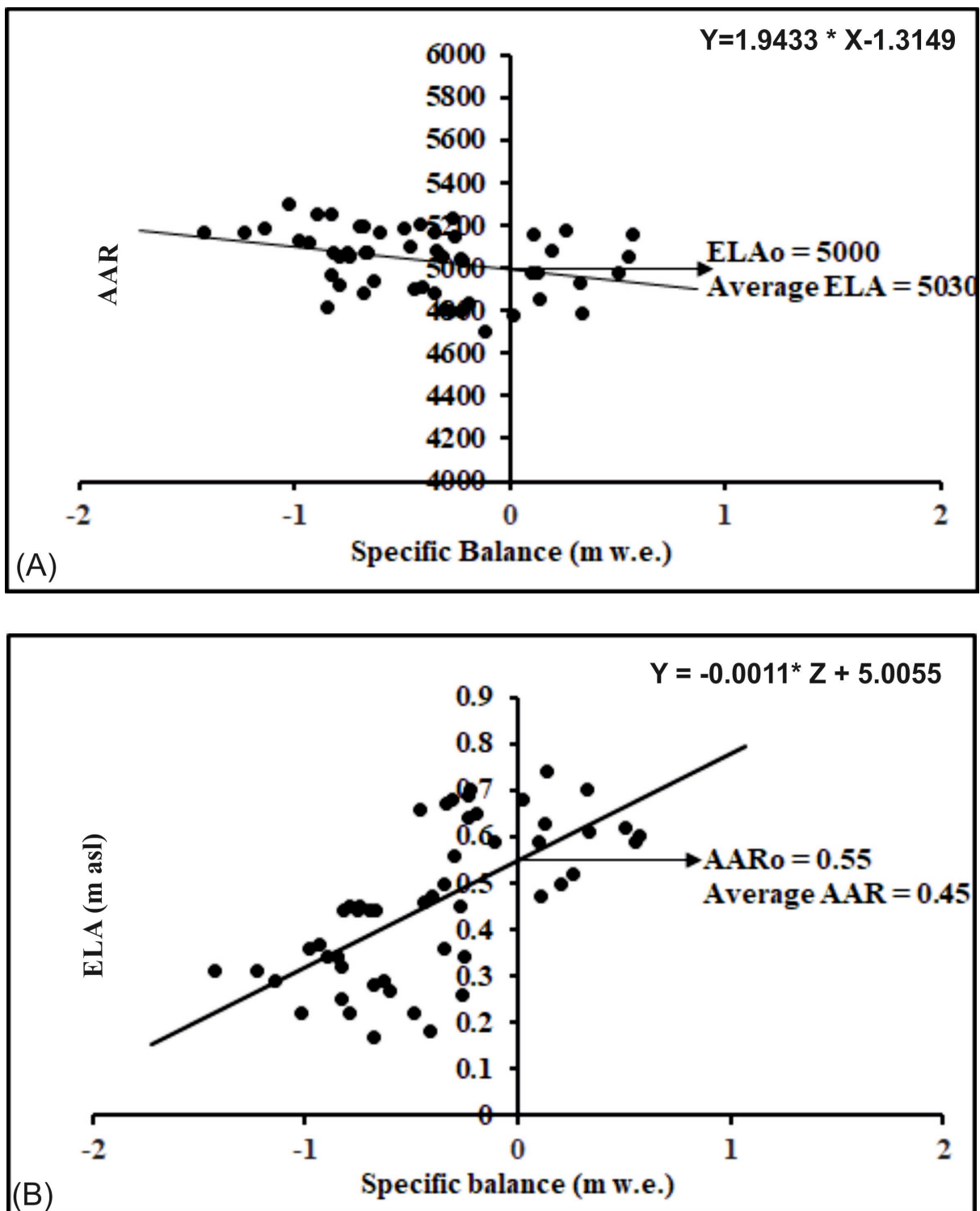


**Figure 5.** (A) The relationship between specific balance and Accumulation Area Ratio (AAR). (B) Relationship between specific balance and Equilibrium Line Attitude (ELA) of Himalayan glaciers. The equilibrium state ELA and AAR is indicated by the intersection of the best-fit line and the vertical axis is specific balance. The ELA and AAR for equilibrium state of the glacier are obtained to be 5000 m asl and 0.55, respectively. Note that 12 years of positive balance occurred in 1975/1976 and 1982/1983 (Gara Glacier), 1982/1983 (Gor Gorang Glacier), 1983 and 1989 (Shaune Gorang Glacier), and 2005, 2009, 2010, and 2011 (Chota Shigri). The average ELA and AAR of the Himalayan glaciers is about 5030 and 0.45, respectively between 1975 and 2011.

The longitudinal profile to estimate the surface elevation change is constructed by using SRTM version -3 (v3) of 2000 and ASTER DEM of 2017 (Figure 6). The surface elevation change was measured using the longitudinal profile of two periods (2000 and 2017). The longitudinal profiles along the centerline of the glacier were drawn and compared. After comparing these two longitudinal profiles, surface lowering was measured in an Excel spreadsheet that helped to compare these two longitudinal profiles; surface lowering was measured in an Excel spreadsheet that helped estimate the thickness loss by the glaciers between 2000 and 2017. For a generation of ASTER DEMs 2017, we adopted the method of Garg et al. [28] using the stereo pair bands: 3N (nadir-looking) and 3B (backward-looking). This process involved inputting ground control points, generation of tie points, creation of epipolar images, image matching, and DEM geocoding. With SRTM DEM as vertical and Sentinel MSI as horizontal references, nearly ten ground control points were collected mainly from stream confluence, glacier peaks, mountain ridges, permanent boulders, or any other prominent feature for enhancing the accuracy of the DEMs. Nearly 97 tie points were used to generate the epipolar images (right and left), obtaining a y-parallax of 1.8 in 2017. Finally, the output DEMs were extracted at 30 m spatial resolution, possessing high terrain details (level 4). The DEMs were then edited using the spline method and median filter with kernel size  $5 \times 5$  to rectify the unnatural peaks and void and smoothen the DEMs. The generated DEMs covered the entire glacier; however, they comprised certain voids (data gaps) primarily due to cloud or snow cover and shadowed regions. The DEM co-registration (horizontal and vertical adjustments) and surface elevation change were estimated by Garg et al. [28].

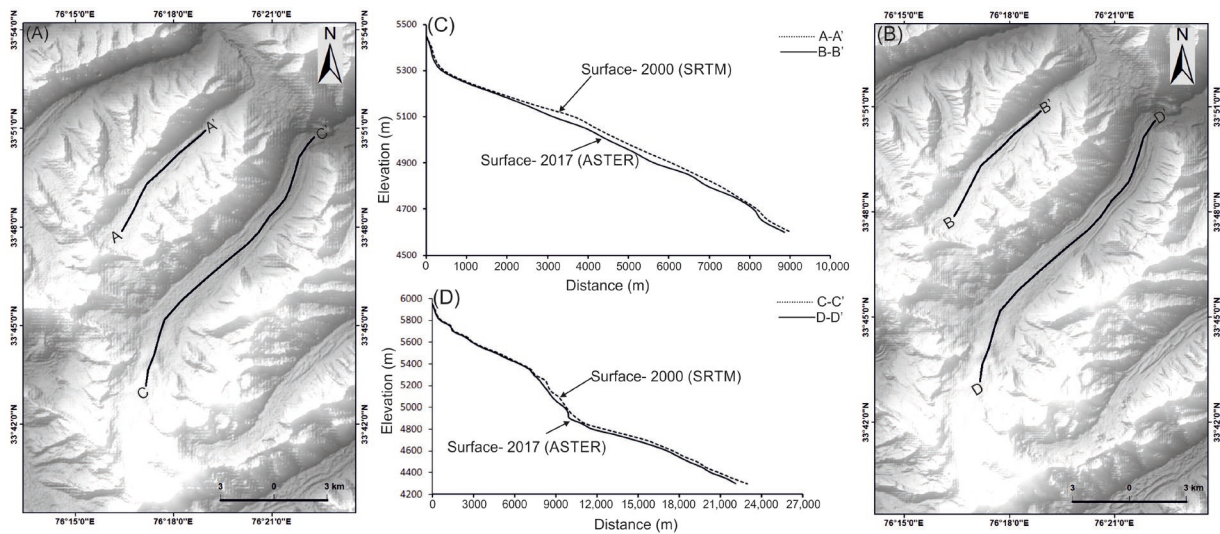


**Figure 6.** Surface elevation change of the PG and DDG along the centerline (AA' and BB' for PG and CC' and DD' for DDG) at different times. (A) SRTM DEM (2000) and (B) ASTER DEM (2017). The methodology of the surface elevation change is discussed in the text. The longitudinal profile along the centerline of the (C) PG and (D) DDG, showing the elevation change between 2000 and 2017.

### 3. Results

#### 3.1. Terminus Retreat and Area Changes

The terminus retreat and area change of PG between 1971 and 2019 is divided into three categories: (i) remote sensing-based total terminus retreat from 1971 to 2019 was  $\sim 270 \pm 27$  m at an average rate of  $5.6 \pm 0.57$  m a<sup>-1</sup>, (ii) Google Earth-based total terminus retreat from 2004 to 2017 was  $\sim 110.5 \pm 18.25$  m at the average rate of  $7.4 \pm 1.23$  m a<sup>-1</sup> and (iii) field observations from 2015 to 2019 with glacier retreat of  $\sim 27 \pm 11.5$  m at an average rate of  $6.7 \pm 3$  m a<sup>-1</sup>. Overall, the glacier lost about 3% of its total length (Figure 4; Table 4).

**Table 4.** Frontal retreat of DDG and PG glaciers between 1971 and 2019.

Glacier Name	Periods	Years	Total Retreat (−)/Advance (+) (m)	Rate (m a <sup>−1</sup> )
Durung Drung	1971–1977	6	(−) 37 ± 20	(−) 6 ± 3
	1977–1994	17	(−) 220 ± 200	(+) 13 ± 12
	1994–2002	8	(−) 118 ± 107	(−) 15 ± 13
	2002–2019	17	(−) 249 ± 220	(−) 115 ± 13
Total	-	48	(−) 624 ± 547	(−) 13 ± 11
Pensilungpa	1971–1977	6	(−) 27 ± 2	(−) 4.5 ± 0.3
	1977–1994	17	(−) 94.5 ± 10	(+) 5.5 ± 0.6
	1994–2002	8	(−) 45 ± 4	(−) 5.6 ± 0.5
	2002–2019	17	(−) 104 ± 11	(−) 6 ± 0.6
Total	-	48	(−) 270.5 ± 27	(−) 5.6 ± 0.56

The area loss by the PG in its pro-glacial region for the period between 1971 and 2019 was  $\sim(-) 1.5 \pm 0.02 \text{ km}^2$  (8% of total area), an average rate of  $(-) 0.03 \pm 0.004 \text{ km}^2 \text{ a}^{-1}$ , out of which  $\sim(-) 0.09 \pm 0.07 \text{ km}^2$  was frontal area loss. The measured field data suggested that the glacier lost  $\sim 1043 \pm 179 \text{ m}^2$  ( $0.0010 \text{ km}^2$ ) in the proglacial area between 2015 and 2019.

The frontal geometry of the DDG is very peculiar, and it appears like a colossal lobe. The glacier's snout is very broad, approximately 2.0 km wide (Figure 4). Due to the large extension of the terminus, the retreat of the glacier snout is reflected as oscillation or quasi-stagnant. The broad snout of the DDG creates wide discrepancies for the frontal retreat. The left part (NW) of the glacier retreat was  $\sim 576 \text{ m}$ , and the right part (NE) of the glacier retreat was  $\sim 104 \text{ m}$ , while, at the same time, the center part of the glacier retreat was  $\sim 1195 \text{ m}$  between 1971 and 2019. The estimation from Google Earth shows that the DDG retreated by  $\sim 227 \pm 131 \text{ m}$  with an average rate of  $17.46 \pm 10 \text{ m a}^{-1}$  between 2004 and 2017. Further, the field observation suggests that the DDG retreated  $\sim 61.5 \pm 33 \text{ m}$  with an average rate of  $15.4 \pm 8 \text{ m a}^{-1}$  from 2015 to 2019. Overall, the DDG reduced  $\sim(-) 624 \pm 547 \text{ m}$  length with an average rate of  $\sim(-) 12 \pm 11 \text{ m a}^{-1}$  which is  $\sim 3\%$  of the total length in the last 48 years (Figure 4).

During the study period, the DDG lost  $\sim 7.78 \pm 0.05 \text{ km}^2$  area (10% of total area) with a rate of  $\sim 0.16 \pm 0.001 \text{ km}^2 \text{ a}^{-1}$ , out of which  $0.91 \pm 0.07 \text{ km}^2$  was the frontal area (which is 12% of the total area lost).

### 3.2. Equilibrium Line Altitude (ELA) and Accumulation Area Ratio (AAR) Changes

The results of ELA and AAR estimated for DDG and PG, based on AAR, THAR, AABR, and MELM methods, are presented in Table 5. It shows that the ELA of DDG and PG in 1971 was at  $\sim 5192 \pm 29$  and  $5198 \pm 23 \text{ m asl}$ , respectively, while the AAR of the glacier was  $\sim 0.54$  for DDG and  $\sim 0.51$  for PG. The terminus of the DDG and PG was located at the altitude of 4090 and 4610 m asl in 1971, respectively. Between 1971 and 2019 (48 years), the ELA of DDG and PG ascended by  $\sim 59 \pm 38$  and  $\sim 23 \pm 19 \text{ m}$ , respectively. The recent ELA of the glaciers is located at the  $\sim 5251 \pm 52$  (DDG) and  $5221 \pm 31 \text{ m asl}$  (PG), respectively (Table 5). Moreover, the estimated AAR is  $\sim 0.46$  for the DDG and  $\sim 0.43$  for the PG in 2019. An in situ study of PG suggested that the ELA of the glacier fluctuated between 5215 and 5223 m asl between 2016 and 2019, and the mean ELA of the glacier was at 5221 m asl [5]. The 2019 estimated ELA of PG is well correlated with the in situ (calculated) ELA.

### 3.3. Volume Loss by the Glaciers

The total ice volume of DDG and PG glaciers is derived from six approaches and presented in Table 6. The calculated volume of the DDG glacier was  $1.42 \times 10^{10} \pm 0.38 \times 10^{10} \text{ m}^3$  in 1971, which was reduced by  $\sim 12\%$  and remained at  $1.25 \times 10^{10} \pm 0.34 \times 10^{10} \text{ m}^3$  in 2019 (Table 6).

**Table 5.** Estimated ELAs, ELAs changes, and AAR of the DDG and PG glaciers between 1971 and 2019.

Glacier Name	Year	AAR (0.45, 0.55, 0.65)	THAR (0.5, 0.6)	AABR	MELM	Average	AAR
Durung Drung	1971	5145	5212	5119	5220	5192 ± 29	0.54
	2002	5176	5217	5223	5260	5219 ± 30	0.49
	2019	5204	5228	5233	5340	5251 ± 52	0.46
						ΔELA = 59 ± 38	
Pensilungpa	1971	5164	5203	5228	5200	5198 ± 23	0.51
	2002	5169	5211	5229	5250	5214 ± 30	0.46
	2019	5173	5218	5239	5255	5221 ± 31	0.43
						ΔELA = 23 ± 19	

**Table 6.** Estimated volume of DDG and PG glaciers between 1971 and 2019.

Glacier Name	Years	Area (m <sup>2</sup> )	$hf = \frac{\tau}{\rho_{ice} g \sin(\sigma)}$ (m <sup>3</sup> )	$V = c A^\gamma$ (m <sup>3</sup> )					Average (m <sup>3</sup> )	SD
				$c = 0.1910$ $\gamma = 1.375$	$c = 0.2055$ $\gamma = 1.36$	$c = 0.8433$ $\gamma = 1.3$	$c = 0.2800$ $\gamma = 1.375$	$c = 0.2100$ $\gamma = 1.35$		
Durung Drung	1971	82.2 × 10 <sup>6</sup>	1.1 × 10 <sup>10</sup>	1.45 × 10 <sup>10</sup>	1.19 × 10 <sup>10</sup>	1.64 × 10 <sup>10</sup>	2.14 × 10 <sup>10</sup>	1.02 × 10 <sup>10</sup>	1.42 × 10 <sup>10</sup>	0.38 × 10 <sup>10</sup>
	2019	75 × 10 <sup>6</sup>	0.9 × 10 <sup>10</sup>	1.29 × 10 <sup>10</sup>	1.05 × 10 <sup>10</sup>	1.45 × 10 <sup>10</sup>	1.87 × 10 <sup>10</sup>	0.89 × 10 <sup>10</sup>	1.25 × 10 <sup>10</sup>	0.34 × 10 <sup>10</sup>
Total Loss	-	7.5 × 10 <sup>6</sup>	0.15 × 10 <sup>10</sup>	0.18 × 10 <sup>10</sup>	0.15 × 10 <sup>10</sup>	0.19 × 10 <sup>10</sup>	0.26 × 10 <sup>10</sup>	0.12 × 10 <sup>10</sup>	0.18 × 10 <sup>10</sup>	0.05 × 10 <sup>10</sup>
Pensilungpa	1971	16.2 × 10 <sup>6</sup>	0.18 × 10 <sup>10</sup>	0.16 × 10 <sup>10</sup>	0.13 × 10 <sup>10</sup>	0.2 × 10 <sup>10</sup>	0.23 × 10 <sup>10</sup>	0.11 × 10 <sup>10</sup>	0.17 × 10 <sup>10</sup>	0.04 × 10 <sup>10</sup>
	2019	13.5 × 10 <sup>6</sup>	0.16 × 10 <sup>10</sup>	0.12 × 10 <sup>10</sup>	0.10 × 10 <sup>10</sup>	0.16 × 10 <sup>10</sup>	0.18 × 10 <sup>10</sup>	0.09 × 10 <sup>10</sup>	0.14 × 10 <sup>10</sup>	0.03 × 10 <sup>10</sup>
Total Loss	-	2.7 × 10 <sup>6</sup>	0.13 × 10 <sup>10</sup>	0.04 × 10 <sup>10</sup>	0.03 × 10 <sup>10</sup>	0.04 × 10 <sup>10</sup>	0.05 × 10 <sup>10</sup>	0.02 × 10 <sup>10</sup>	0.03 × 10 <sup>10</sup>	0.01 × 10 <sup>10</sup>

Similarly, the ice volume of the PG glacier was estimated as  $\sim 0.17 \times 10^{10} \pm 0.04 \times 10^{10} \text{ m}^3$  in 1971 and  $0.14 \times 10^{10} \pm 0.03 \times 10^{10} \text{ m}^3$  in 2019. Between 1971 and 2019, the glacier lost about  $0.03 \times 10^{10} \pm 0.01 \times 10^{10} \text{ m}^3$ , about 17% of the total volume.

### 3.4. Glacier Mass Balance and Thickness Change

We used the AAR/ELA method to estimate the glacier mass balance rate (specific balance) of DDG and PG for the years 1971, 2002, and 2019. The result shows the continuous mass loss since 1971 (Table 7). The modeled average specific balance of the DDG was  $-0.29 \pm 0.33 \text{ m w.e.}$  for 1971,  $-0.37 \pm 0.29 \text{ m w.e.}$  for 2002, and  $-0.42 \pm 0.28 \text{ m w.e.}$  for 2019, whereas the estimated specific mass balance of PG was  $-0.33 \pm 0.31 \text{ m w.e.}$  for 1971,  $-0.41 \pm 0.26 \text{ m w.e.}$  for 2002, and  $-0.45 \pm 0.23 \text{ m w.e.}$  for 2019.

**Table 7.** Modeled mass balance of DDG and PG glaciers between 1971 and 2019.

Glacier Name	Year	Specific Mass Balance (m w.e.)			Average
		$Spb = 2.4301 \times$ $AAR - 1.20187$	$Spb = 1.9433 \times$ $AAR - 1.3149$	$Spb = -0.0011 \times$ $ELA + 5.0055$	
Durung Drung	1971	+0.11	-0.27	-0.71	$-0.29 \pm 0.33$
	2002	-0.01	-0.36	-0.73	$-0.37 \pm 0.29$
	2019	-0.08	-0.42	-0.77	$-0.42 \pm 0.28$
Average mass balance = $-0.36 \pm 0.3$					
Pensilungpa	1971	+0.04	-0.32	-0.71	$-0.33 \pm 0.31$
	2002	-0.08	-0.42	-0.73	$-0.41 \pm 0.26$
	2019	-0.16	-0.48	-0.74	$-0.45 \pm 0.23$
Average mass balance = $-0.4 \pm 0.27$					

A recent study by Mehta et al. [5] based on glaciological mass balance suggested that the average specific balance of PG was  $-0.36 \text{ m w.e. a}^{-1}$  during the periods 2016/2017–2018/2019. The mass wastage rate in the ablation zone is about  $0.82 \text{ m w.e. a}^{-1}$ , with the mass gain

in the accumulation area, being about  $0.27 \text{ m w.e. a}^{-1}$  between 2016/2017 and 2018/2019. The modeled value of the specific mass balance of PG is near to in-situ measurement.

### 3.5. Longitudinal Profiles and Elevation Change

For surface elevation change, a longitudinal profile along the centerline was drawn between 2000 and 2017 (Figure 6). The longitudinal profile shift between 2000 and 2017 shows that PG lost  $\sim 15 \text{ m}$  surface ice thickness, while DDG lost  $\sim 17 \text{ m}$  ice thickness (Table 8). The PG lost maximum thickness between 5100 and 4900 m asl, where the debris thickness is  $< 5 \text{ cm}$ , while the minimum thickness was lost between 4800 and 4700 m where the debris thickness was  $> 10 \text{ cm}$  (Table 8). However, between 4750 and 4700 m asl, no loss in ice thickness was observed. Compared to PG (thick debris-covered) and DDG (thin debris-covered), the ice thickness loss on the centerline shows linear trends except for some places (Figure 6). The upper ablation zone (4950–5150 m asl) of DDG lost higher ice thickness (average  $-23 \text{ m}$ ), while the lower ablation zone (4700–4900 m asl) lost less ice thickness (average  $-10 \text{ m}$ ), whereas DDG showed linearity with ice thickness loss, except in some places between 4950 and 5000 m asl (Figure 6). Generally, melting at lower elevations is higher than in the upper areas; at PG, that is not the case, probably due to the thick debris cover. The elevation-wise thickness lost by the glaciers is presented in Table 8 and Figure 6.

Table 8. The elevation-wise thickness lost by the glaciers.

Pensilungpa Glacier			Durung Drung		
Elevation Range (m a.s.l.)	Ice Thickness Lost (m)	SD	Elevation Range (m a.s.l.)	Ice Thickness Lost (m)	SD
5200–5150	5	2	5350–5250	5	1.5
5150–5050	25	12	5250–5150	20	9
5050–4950	18	10	5150–5000	20	13
4950–4900	25	13	5000–4950	7	2
4900–4800	15	7	4950–4800	25	13
4800–4700	5	3	<4800	25	14
<4700	10	6			
Average thickness lost	14.71	8		17	9

## 4. Discussion

The glaciers' response to ongoing climate change across the Himalayas is complicated to understand due to the complex topography and lack of systematic or long-term field measurements. Within each of the individual mountain ranges, the large amount of scattering in the pattern of relative changes suggests that the local factors are essential in controlling the behavior of the glaciers. These may include differences in local climatic history and/or differences in the intrinsic sensitivity of the glaciers to climatic change as a result of differences in slope [69–71], aspect, elevation, hypsometry, and presence of debris cover [72] or rate of mass turnover [73,74]. Similar patterns have been observed in the Himalayan region [18,75–80]; however, these studies have reported that the smaller glaciers' loss is much faster than the larger ones. The DDG and PG are located in the same climatic regime and flow in the same direction (NNE). The geomorphological evidence suggests that these two glaciers were connected in the past, but now they are dispersed in different directions [30]. Geometrically and morphologically, the DDG and PG are different, DDG has a thin debris cover (only 5.5% area) and is the biggest glacier in the basins (Doda and Suru), having a broader snout ( $\sim 2 \text{ km}$ ). DDG ( $72 \text{ km}^2$ ) is five times bigger than the PG ( $16 \text{ km}^2$ ), and both glaciers reduced in length  $\sim 624 \pm 547$  and  $270 \pm 27 \text{ m}$  with the rate of  $12 \pm 11$  and  $5.6 \pm 0.5 \text{ m a}^{-1}$  between 1971 and 2019, respectively. The PG has lost its length at a two times slower rate than the DDG, while both glaciers lost a similar percentage of the length, which is  $\sim 3\%$  of the total length. This comparative study shows that the thick debris-covered ablation front of PG retreats more slowly, whereas the thin debris-covered DDG front retreats at a faster rate. Scherler et al. [21] suggested that the glacier retreat

rate varies with >20% debris cover zero, whereas it is high for the debris-free glacier. This can be correlated with the influence of debris (>17%) over PG with a slower retreat rate compared to DDG with less (5.5%) debris cover. A debris cover influences the terminus dynamics and modifies a glacier's response to climate change [21]. Surface ablation rates are generally increased in the presence of a thin (<5 cm) debris cover but are significantly reduced when a thick (>5 cm) debris cover is present [5,10,15,21]. Thin and patchy debris cover reduces the albedo and elevates shortwave radiation absorption, whereas ablation rates are strongly reduced further down the glacier due to the insulating effect of thicker debris [10,20]. Additionally, we observed that the broad front of the DDG indicates the oscillatory nature. The left and central parts of the glacier lost higher length, but the right part of the snout is quasi-stagnant (Figure 3). Due to the oscillatory nature, the center part of the snout of the DDG advanced  $33 \pm 12$  m between 2013 and 2017, whereas the glacier shows high uncertainty and a total retreat of  $\sim 36 \pm 60$  m in the same periods (2013–2017).

An earlier study by Shukla and Qadir [81] suggested that the retreat of DDG was  $\sim 691$  m and PG was  $\sim 298$  m between 1977 and 2013 with an average rate of  $\sim 19$  and  $\sim 8$  m  $a^{-1}$ , respectively. Similarly, Kamp et al. [24] suggested that the retreat of DDG was  $\sim 311$  m with an average rate of  $\sim 9$  m  $a^{-1}$  between 1975 and 2008. However, the retreat of PG was  $\sim 1887$  m, with the average rate of the retreat being  $\sim 61$  m  $a^{-1}$  between 1975 and 2006 [24]. Similarly, a recent study by Rashid and Majeed [82] shows that the DDG retreated 925 m at the rate of 20 m  $a^{-1}$  between 1971 and 2017; it seems that the authors took the recession from the center of the snout. In comparison, our study suggested that the snout of DDG retreated  $\sim 576$  m from the left side (NW),  $\sim 104$  m from the right part (NE), and  $\sim 1195$  m from the center part of the glacier between 1971 and 2019. The present study suggests that the center part of the snout of the DDG advanced between 2013 and 2017, whereas the PG was in continuous retreat.

Lee et al. [13] studied >14,000 glaciers in the Himalayas and suggested that the Himalayan glaciers lost 40% of their area between LIA (400 to 700 years ago) and recent years. Mehta et al. [5] studied the PG between the same period of LIA (400 and 700 years ago and recent years) and suggested that glaciers lost 16% of their total area and 27% of their total length based on the field data. The comparative studies showed that PG lost a lower percentage of the area. Lee et al. [13] also indicated that the ranges of mass loss rate of the Himalayan glaciers between LIA and the recent year were  $-0.011$  and  $-0.020$  m w.e.  $a^{-1}$ , which was a lower rate than current trends. Maurer et al. [12] estimated the mass balance of the Himalayan glaciers and suggested that the average mass balance rate of the Himalayan glaciers was  $-0.33 \pm 0.13$  m w.e.  $a^{-1}$  between 1975 and 2016. The present study based on ELA and AAR model suggested that the modeled mass balance rate of DDG is  $-0.36 \pm 0.3$  m w.e.  $a^{-1}$  and PG is  $-0.39 \pm 0.26$  m w.e.  $a^{-1}$  between 1971 and 2019. DDG and PG lost 12% and 17% of ice volume during the same periods, respectively. The in situ mass balance study of PG shows a rate of  $-0.36$  m w.e.  $a^{-1}$  between 2016 and 2019, which supports the result of the estimated mass balance rate ( $-0.39 \pm 0.26$  m w.e.  $a^{-1}$ ) of the PG glacier by Mehta et al. [5]. The ELA and AAR-based mass balance of the DDG and PG is well correlated with the modeled and in situ mass balance of the Himalayan glaciers. The in situ mass balance rate of the Dokriani (Uttarakhand), Chhota Shigri (Himachal Pradesh), Pokalade (Nepal), and Pensilungpa (Zaskar, Ladakh) is  $-0.69$ ,  $-0.32$ ,  $-0.56$ , and  $-0.36$  m w.e.  $a^{-1}$ , respectively [5,10,83,84], whereas the remote sensing and geodetic-based studies suggested that the mass balance rate across the Himalaya was  $-0.33 \pm 0.13$  m w.e.  $a^{-1}$  between 1975 and 2016 [12], the Himalayan sub-region was  $-0.35$  m w.e.  $a^{-1}$  between 1999 and 2008 [85], Hindu Kush–Karakoram–Himalaya region (HKKH) was  $-0.21 \pm 0.05$  m w.e.  $a^{-1}$  between 2003 and 2008 [86], High Mountain Asia lost ice with the rate of  $-0.34 \pm 0.06$  m w.e.  $a^{-1}$  between 2000 and 2016 [26]. However, Garg et al. [87] suggested that the average mass balance of the glaciers in the Suru River basin was  $-0.69$  m w.e.  $a^{-1}$ , which is higher than the present study. The ELA and AAR-based mass balance of DDG and PG are well correlated with above mentioned in situ (glaciological) and remote sensing (geodetic) based mass balance studies.

The effect of atmospheric warming has upwardly shifted the ELA, increasing the ablation area of the Himalayan glaciers [5,10,88–91]. The ELA of thin debris-covered Gara Glacier ascended ~108 m between 1975 and 1983, and the average AAR of the glacier was ~0.41, while the ELA of clean Gor Garang Glacier shifted ~30 m in seven years (1977–1984) and the average AAR of the glacier was ~0.32 m [11,92–94]. Furthermore, the ELAs of thick debris-covered Shaune Garang and thin debris-covered Chhota Shigri glaciers have shown a higher shift with ~160 m (AAR ~0.43) between 1982 and 1991 (10 years) and 373 m (AAR ~0.52) between 1987 and 2011 (25 years), respectively [11,94–96]. Moreover, the ELAs of thick debris-covered Naradu (2001–2003), clean Rulung (1980–1981), and thick debris-covered Dunagiri (1985–1990) glaciers shifted ~10, 25, and 27 m with average AARs of ~0.48, ~0.43, and ~0.14, respectively [97–99]. Similarly, clean Dokriani, thick debris-covered Chorabari, and Bangni glaciers shifted ELAs ~48, 15, and 64 m during 1993–2013, 2004–2010, and 1962–2013, respectively [10,18,38]. The AAR of Dokriani Glacier was ~0.67 between 1993 and 2013, while the AAR of the Chorabari Glacier was ~0.44 between 2004 and 2013 [10,18,91]. The above observations are compared with the present study, and suggests that the ELA of the DDG and PG shifted by  $59 \pm 38$  and  $23 \pm 19$  m between 1971 and 2019, respectively. However, the estimated AARs of DDG and PG were ~0.46 and ~0.43 in 2019, respectively. The in situ study by Mehta et al. [5] suggested that the ELA of the PG glacier shifted ~8 m, and the average AAR of the glacier was 0.43 between 2016 and 2019. These studies reflected that the ELA of the Central and Western Himalayan glaciers shifted upward and the present ELA is located between 5000 and 5250 m asl, which shows that the glaciers are continuously losing their mass since the early twentieth century.

The combination of continuous retreat in length, reduction in volume, and upward shift of the ELA can be attributed to the rising temperature and changes in precipitation trends in the Himalaya. More definitive connectivity between glacier recession, ELA change, and recent climate change requires a regional-scale study. Nevertheless, as far as the DDG and PG are concerned, if the present climate trend continues, it is expected that the glaciers will continue to decrease in ice volume.

The morphological parameters of these two glaciers (DDG and PG) are different, while the topographical characteristics are almost similar. The rate of area and length loss by the DDG is about eight times higher than the PG. According to CRU-TS 4 meteorological data (1901–2018), both glaciers are located in the same grid and showing that the winter temperature and summer precipitation have increased since 1980 (Figure 2). The difference in glacier recession cannot be well explained by climate records individually. Thus, we calculated the topographical characteristic (slope, aspect, altitude, and size) of both glaciers to track their influences on glacier changes. The average slope of the PG is  $8^\circ$ , and DDG is  $6^\circ$  and both glaciers face the NE direction. The ELA of both glaciers is located at 5221 m asl for PG and 5251 m asl for DDG, while the mean median altitude of the PG is 5320 m asl and DDG is 5250 m asl. Aizen et al. [100] suggested that the melting of the glaciers is driven by solar radiation (up to 86%), based on the meteorological station records. However, Shukla et al. [20] and Kumar et al. [3,18] suggested that the aspects and slope are important factors affecting glacier changes. There is no significant difference in topographic and climate factors between PG and DDG. Thus, we extrapolate that the incoming solar radiation affected by the aspects and slopes cannot cause the difference in glacier changes in Suru and Doda River basins. We find that the DDG ( $72 \text{ km}^2$ ) is bigger than PG ( $16 \text{ km}^2$ ); consequently, we may speculate that different retreat rates of the glaciers are probably caused by the difference in glacier size. The debris thickness could also affect the ablation of glaciers [101–103]. The presence of supraglacial debris covers influences glacier processes. Depending on thickness, debris cover may either enhance or retard the ablation process [10,20,21]. PG covered 17% ( $1.8 \text{ km}^2$ ) of their area with debris, while the DDG covered 5.5% ( $3.8 \text{ km}^2$ ) of the area with debris. We observed during the period between 2015 and 2019 that the lower ablation zone of the PG is covered by thick debris and reduces the frontal retreat of the glacier, whereas the lower ablation zone of the DDG is covered by thin or scattered debris and enhances the frontal retreat of the glaciers. The

supraglacial ponds/lakes and proglacial lakes act as ablation hotspots and increase the ablation rate of the glacier [81,104,105]. Two large proglacial lakes format the front of the DDG, covering an area of about 2 km<sup>2</sup>. Due to the proglacial lake, the snout of the DDG retreats faster than PG, and the ice of the margin of the snout breaks continuously. Although we cannot find a strong correlation between glacier retreat, meteorology, and topography factors, both glaciers are located in the same climatic zone, aspect, and slope. Nevertheless, we expect that the glacier size, debris cover, and glacier lake probably influence the rate of glacier retreat in the Suru and Doda River basins.

## 5. Conclusions

In this study, we present the result of length, area, ELA, volume, and mass balance changes of two glaciers (DDG and PG) located in the Doda and Suru River basins. The DDG and PG are located in the same climatic zone, aspect, and slope. Nevertheless, there is a lot of heterogeneity in the recession patterns of both glaciers. The DDG lost an area of 7.78 km<sup>2</sup> (10% of the total area) which was five times higher than PG (1.5 km<sup>2</sup>; 8% of the total glacier area). The retreat rate of the DDG is 13 m a<sup>-1</sup> between 1971 and 2019, which is two times higher than the PG (5.6 m a<sup>-1</sup>).

Moreover, the ELA of DDG shifted 59 m upward between 1971 and 2019, while the ELA of PG shifted 23 m in the same period. However, the ELA of both glaciers was located in the same altitude zone (5200–5300 m asl) in 2019. We expect that the glacier size, debris cover, and glacier lake probably influenced the rate of glacier retreat in the Suru and Doda River basins. This trend in glacier retreat rates over time is similar to that for other glaciers in the western, central, and eastern Himalayas. The increase in temperature and reduction in precipitation mainly causes the retreat of the glaciers. The increasing amount of precipitation could not compensate for the glacier mass loss due to the temperature increase in Zaskar Himalaya (Suru and Doda basins). This suggested that the warming of the climate is also responsible for the glacier retreat in the study area. The rate of glacier retreat is not only controlled by climate change but also by the topographic setting and morphology of the glacier. The comparative study also confirms the possible influence of factors such as snout geometry, glacier size, elevation range, slope, aspect, debris cover, and presence of supra and proglacial lakes other than the climate in the observed heterogeneous response of the studied glaciers. Therefore, these factors need to be accounted for in more detail in future studies for a complete understanding of the observed glacier changes and responses.

**Author Contributions:** M.M. and V.K. conceived the idea, designed the study, and wrote the manuscript. M.M., V.K. and P.K. carried out the fieldwork. K.S. reviewed and finalized the structure of the manuscript. All authors have read and agreed to the published version of the manuscript.

**Funding:** This research received no external funding.

**Institutional Review Board Statement:** Not applicable.

**Informed Consent Statement:** Not applicable.

**Data Availability Statement:** Available on MDPI site.

**Acknowledgments:** The authors are grateful to the Director of Wadia Institute of Himalayan Geology (WIHG), Dehra Dun, India, for providing facilities and ample support to carry out this work. We are also thankful to the Department of Science and Technology, Ministry of Science and Technology, Government of India for financial support to carry out this work. The authors wish to thank Aparna Shukla (Scientist, Ministry of Earth Sciences, New Delhi) for her help in the field investigation of the glaciers. We especially thank the field party and local people of Parkachik and Rangdum villages, Ladakh, for their assistance during the field campaign.

**Conflicts of Interest:** The authors declare no conflict of interest.

## References

1. Shahgedanova, M.; Stokes, R.C.; Gurney, S.D.; Popovnin, V. Interactions between mass balance, atmospheric circulation, and recent climate change on the Djankuat Glacier, Caucasus Mountains, Russia. *J. Geophys. Res. Atmos.* **2005**, *110*, 1–14. [\[CrossRef\]](#)
2. Paterson, W.S.B. *The Physics of Glaciers*, 3rd ed.; Elsevier: New York, NY, USA, 1994; p. 480.
3. Kumar, V.; Shukla, T.; Mishra, A.; Kumar, A.; Mehta, M. Chronology and climate sensitivity of the Post LGM glaciation in the Dunagiri valley, Dhauliganga basin, Central Himalaya, India. *Boreas* **2020**, *49*, 594–614. [\[CrossRef\]](#)
4. Vinit, K.; Shukla, T.; Mehta, M.; Dobhal, D.P.; Bisht, M.P.S.; Nautiyal, S. Glacier changes and associated climate drivers for the last three decades, Nanda Devi region, Central Himalaya, India. *Quat. Int.* **2021**, *575*, 213–226.
5. Mehta, M.; Kumar, V.; Garg, S.; Shukla, A. Little ice age glacier extent and temporal changes in annual mass balance (2016–2019) of Pensilungpa Glacier, Zaskar Himalaya. *Reg. Environ. Chang.* **2021**, *21*, 38. [\[CrossRef\]](#)
6. Raina, V.K.; Srivastava, D. *Glacier Atlas of India*; Geological Society of India: Bangalore, India, 2008; p. 316.
7. Mayewski, P.A.; Jeschke, P.A. Himalayan and trans-Himalayan glacier fluctuations since A.D 1812. *Arct. Antarct. Alp. Res.* **1979**, *11*, 267–287. [\[CrossRef\]](#)
8. Sakai, A.; Takeuchi, N.; Fujita, K.; Nakawo, M. Role of Supraglacial Ponds in the Ablation Process of a Debris Covered Glacier in the Nepal Himalayas. *Iahs Publ.* **2000**, *265*, 119–130.
9. Casey, K.; Käab, A.; Benn, D. Geochemical characterization of supraglacial debris in situ and optical remote sensing methods: A case study in Khumbu Himalaya, Nepal. *Cryosphere* **2012**, *6*, 85–100. [\[CrossRef\]](#)
10. Dobhal, D.P.; Mehta, M.; Srivastava, D. Influence of debris cover on terminus retreat and mass changes of Chorabari Glacier, Garhwal region, central Himalaya, India. *J. Glaciol.* **2013**, *59*, 961–971. [\[CrossRef\]](#)
11. Pratap, B.; Dobhal, D.P.; Mehta, M. Influence of debris cover and altitude on glacier surface melting: A case study on Dokriani Glacier, central Himalaya, India. *Ann. Glaciol.* **2015**, *56*, 9–16. [\[CrossRef\]](#)
12. Maurer, J.M.; Schaefer, J.M.; Rupper, S.; Corley, A. Acceleration of ice loss across the Himalayas over the past 40 years. *Sci. Adv.* **2019**, *5*, 1–12. [\[CrossRef\]](#)
13. Ethan, L.; Carrivick, J.L.; Quincey, D.J.; Cook, S.J.; James, W.H.M.; Brown, L.E. Accelerated mass loss of Himalayan glaciers since the Little Ice Age. *Sci. Rep.* **2021**, *11*, 1–8.
14. Bozhinskiy, A.N.; Krass, M.S.; Popovnin, V.V. Role of debris cover in the thermal physics of glaciers. *J. Glaciol.* **1986**, *32*, 255–266. [\[CrossRef\]](#)
15. Lundstrom, S.C.; McCafferty, A.E.; Coe, J.A. Photogrammetric analysis of 1984–89 surface altitude changes of the partially debris-covered Eliot Glacier, Mount Hood, Oregon, USA. *Ann. Glaciol.* **1993**, *17*, 167–170. [\[CrossRef\]](#)
16. Bolch, T.; Buchroithner, M.; Pieczonka, T.; Kunert, A. Planimetric and volumetric glacier changes in the Khumbu Himalaya, Nepal, since 1962 using Corona, Landsat TM, and ASTER data. *J. Glaciol.* **2008**, *54*, 592–600. [\[CrossRef\]](#)
17. Schmidt, S.; Nüsser, M. Changes of high-altitude glaciers from 1969 to 2010 in the Trans-Himalayan Kang Yatze massif, Ladakh, Northwest India. *Arct. Antarct. Alp. Res.* **2012**, *44*, 107–121. [\[CrossRef\]](#)
18. Kumar, V.; Mehta, M.; Mishra, A.; Trivedi, A. Temporal fluctuations and frontal area change of Bangni and Dunagiri glaciers from 1962 to 2013, Dhauliganga Basin, central Himalaya, India. *Geomorphology* **2017**, *284*, 88–98. [\[CrossRef\]](#)
19. Mal, S.; Mehta, M.; Singh, R.B.; Schickhoff, U.; Bisht, M.P.S. Recession and morphological changes of the debris-covered Milam Glacier in Gori Ganga Valley Central Himalaya India derived from satellite data. *Front. Environ. Sci.* **2019**, *7*, 42. [\[CrossRef\]](#)
20. Shukla, A.; Garg, S.; Mehta, M.; Kumar, V.; Shukla, U.K. Temporal inventory of glaciers in the Suru sub-basin, western Himalaya: Impacts of the regional climate variability. *Earth Syst. Sci. Data* **2020**, *12*, 1245–1265. [\[CrossRef\]](#)
21. Scherler, D.; Bookhagen, B.; Strecker, M.R. Spatially Variable Response of Himalayan Glaciers to Climate Change Affected by Debris Cover. *Nat. Geosci.* **2011**, *4*, 156–159. [\[CrossRef\]](#)
22. Rowan, A.V.; Egholm, D.L.; Quincey, D.J.; Hubbard, B.; King, O.; Miles, E.S.; Miles, K.E.; Hornsey, J. The role of differential ablation and dynamic detachment in driving accelerating mass loss from a debris-covered Himalayan glacier. *J. Geophys. Res. Earth Surf.* **2021**, *126*, 1–20. [\[CrossRef\]](#)
23. Shukla, A.; Gupta, R.P.; Arora, M.K. Estimation of debris cover and its temporal variation using optical satellite sensor data: A case study in Chenab basin, Himalaya. *J. Glaciol.* **2009**, *55*, 444–452. [\[CrossRef\]](#)
24. Kamp, U.; Byrne, M.; Bolch, T. Mapping glacier fluctuations between 1975 and 2008 in the Greater Himalaya Range of Ladakh, north-western India. *J. Mt. Sci.* **2011**, *8*, 374–389. [\[CrossRef\]](#)
25. Yao, T.; Thompson, L.; Yang, W.; Yu, W.; Gao, Y.; Guo, X.; Yang, X.; Duan, K.; Zhao, H.; Xu, B.; et al. Different glacier status with atmospheric circulations in Tibetan Plateau and surroundings. *Nat. Clim. Chang.* **2012**, *2*, 663. [\[CrossRef\]](#)
26. Brun, F.; Berthier, E.; Wagnon, P.; Käab, A.; Treichler, D. A spatially resolved estimate of high mountain Asia glacier mass balance from 2000 to 2016. *Nat. Geosci.* **2017**, *10*, 468–474. [\[CrossRef\]](#) [\[PubMed\]](#)
27. Bhushan, S.; Syed, T.H.; Arendt, A.A.; Kulkarni, A.V.; Sinha, D. Assessing controls on mass budget and surface velocity variations of glaciers in Western Himalaya. *Sci. Rep.* **2018**, *8*, 8885. [\[CrossRef\]](#)
28. Garg, P.K.; Garg, S.; Yousuf, B.; Shukla, A.; Kumar, V.; Mehta, M. Stagnation of the Pensilungpa glacier, western Himalaya, India: Causes and implications. *J. Glaciol.* **2022**, *68*, 221–235. [\[CrossRef\]](#)
29. Sangewar, C.V.; Shukla, S.P. Inventory of the Himalayan Glaciers: A Contribution to the International Hydrological Programme, An Updated Edition, Kolkata. *Geol. Surv. India Spec. Publ.* **2009**, *34*, 0254–0436.

30. Kumar, V.; Mehta, M.; Shukla, A.; Kumar, A.; Garg, S. Late Quaternary glacial advances and equilibrium-line altitude changes in a semi-arid region, Suru Basin, western Himalaya. *Quat. Sci. Rev.* **2021**, *267*, 107100. [[CrossRef](#)]
31. Harris, I.; Osborn, T.J.; Jones, P.; Lister, D. Version 4 of the CRU TS monthly high-resolution gridded multivariate climate dataset. *Sci. Data* **2020**, *7*, 1–18. [[CrossRef](#)]
32. Bhambri, R.; Bolch, T.; Chaujar, R.K. Frontal recession of Gangotri Glacier, Garhwal Himalayas, from 1965 to 2006, measured through high-resolution remote sensing data. *Curr. Sci.* **2012**, *102*, 489–494.
33. Shukla, A.; Garg, P.K. Evolution of a debris-covered glacier in the western Himalaya during the last four decades (1971–2016): A multiparametric assessment using remote sensing and field observations. *Geomorphology* **2019**, *341*, 1–14. [[CrossRef](#)]
34. Shukla, A.; Garg, S.; Kumar, V.; Mehta, M.; Shukla, U.K. Sensitivity of glaciers in Part of the Suru River valley, Western Himalaya to ongoing climatic perturbations. In *Himalayan Weather and Climate and Their Impact on the Environment*; Springer International Publishing: New York, NY, USA, 2020; pp. 351–377.
35. Garg, S.; Shukla, A.; Mehta, M.; Kumar, V.; Samuel, S.A.; Bartarya, S.K.; Shukla, U.K. Field evidence showing rapid frontal degeneration of the Kangriz glacier, western Himalayas, Jammu & Kashmir. *J. Mt. Sci.* **2018**, *15*, 1199–1208.
36. Garg, S.; Shukla, A.; Mehta, M.; Kumar, V.; Shukla, U.K. On geomorphic manifestations and glaciation history of the Kangriz glacier, western Himalaya. *Himal. Geol.* **2019**, *40*, 115–127.
37. Azam, M.F.; Wagnon, P.; Vincent, C. Reconstruction of the annual mass balance of Chhota Shigri glacier, Western Himalaya, India, since 1969. *Ann. Glaciol.* **2014**, *55*, 69–80. [[CrossRef](#)]
38. Dobhal, D.P.; Pratap, B.; Bhambri, R.; Mehta, M. Mass balance and morphological changes of Dokriani Glacier (1992–2013), Garhwal Himalaya, India. *Quat. Sci. Adv.* **2021**, *4*, 100033. [[CrossRef](#)]
39. Meier, M.F.; Post, A.S. Recent variations in mass net budgets of glacier in western North America. In *Symposium of Oberurgl, Tyrol, Austria, 10 September 1962*; International Association of Scientific Hydrology: Wallingford, UK, 1962; Volume 58, pp. 63–77.
40. Benn, D.I.; Owen, L.A.; Osmaston, H.A.; Seltzer, G.O.; Porter, C.S.; Mark, B. Reconstruction of equilibrium-line altitudes for tropical and sub-tropical glaciers. *Quat. Int.* **2005**, *138–139*, 8–21. [[CrossRef](#)]
41. Mehta, M.; Dobhal, D.P.; Bhanu, P.; Majeed, Z.; Gupta, A.K.; Srivastava, P. Late Quaternary glacial advances in the Tons River Valley, Garhwal Himalaya, India and regional synchronicity. *Holocene* **2014**, *24*, 1336–1350. [[CrossRef](#)]
42. Shukla, T.; Mehta, M.; Jaiswal, M.K.; Srivastava, P.; Dobhal, D.P.; Nainwal, H.C.; Singh, A.K. Late Quaternary glaciation history of monsoon-dominated Dingad basin, central Himalaya, India. *Quat. Sci. Rev.* **2018**, *181*, 43–64. [[CrossRef](#)]
43. Meierding, T.C. Late Pleistocene glacial equilibrium line altitudes in the Colorado Front Range: A comparison of methods. *Quat. Res.* **1982**, *18*, 289–310. [[CrossRef](#)]
44. Osmaston, H. Estimates of glacier equilibrium line altitudes by the Area X Altitude, the Area X Altitude Balance Ratio and the Area X Altitude Balance Index methods and their validation. *Quat. Int.* **2005**, *138–139*, 22–31. [[CrossRef](#)]
45. Sharma, M.C.; Owen, L.A. Quaternary glacial history of the NW Garhwal, central Himalayas, India. *Quat. Sci. Rev.* **1996**, *15*, 335–365. [[CrossRef](#)]
46. Furbish, D.J.; Andrews, J.T. The use of hypsometry to indicate long-term stability and response of valley glaciers to changes in mass transfer. *J. Glaciol.* **1984**, *30*, 199–211. [[CrossRef](#)]
47. Kaser, G.; Osmaston, H. *Tropical Glaciers*; Cambridge University Press: Cambridge, UK, 2002; p. 207.
48. Benn, D.I.; Lehmkuhl, F. Mass balance and equilibrium-line altitudes of glaciers in high mountain environments. *Quat. Int.* **2000**, *65–66*, 15–29. [[CrossRef](#)]
49. Richards, B.W.M.; Owen, L.A.; Rhodes, E.J. Asynchronous glaciation at Naga Parbat, northwestern Himalaya Mountains, Pakistan: Comment. *Geology* **2001**, *29*, 287. [[CrossRef](#)]
50. Porter, S.C. Snowline depression in the tropics during the last glaciation. *Quat. Sci. Rev.* **2001**, *20*, 1067–1091. [[CrossRef](#)]
51. Liu, S.; Sun, W.; Shen, Y.; Li, G. Glacier changes since the Little Ice Age maximum in the western Qilian Shan, northwest China, and consequences of glacier runoff for water supply. *J. Glaciol.* **2003**, *49*, 117–124. [[CrossRef](#)]
52. Cogley, J.G. Present and future states of Himalaya and Karakoram glaciers. *Ann. Glaciol.* **2011**, *52*, 69–73. [[CrossRef](#)]
53. Frey, H.; Machguth, H.; Huss, M.; Huggel, C.; Bajracharya, S.; Bolch, T.; Stoffel, M. Estimating the volume of glaciers in the Himalayan–Karakoram region using different methods. *Cryosphere* **2014**, *8*, 2313–2333. [[CrossRef](#)]
54. Mool, P.K.; Bajracharya, S.R.; Joshi, S.P. Inventory of Glaciers. In *Glacial Lakes and Glacial Lake Outburst Floods—Nepal*; ICIMOD: Kathmandu, Nepal, 2006.
55. Bajracharya, S.R.; Shrestha, B.R. *The Status of Glaciers in the Hindu Kush-Himalayan Region*; International Centre for Integrated Mountain Development (ICIMOD): Kathmandu, Nepal, 2011.
56. Chen, J.; Ohmura, A. *Estimation of Alpine Glacier Water Resources and Their Change Since the 1870s*; IAHS Publication: Wallingford, UK, 1990; Volume 193, pp. 127–135.
57. Bahr, D.B.; Meier, M.F.; Peckham, S.D. The physical basis of glacier volume-area scaling. *J. Geophys. Res. Solid Earth* **1997**, *102*, 20355–20362. [[CrossRef](#)]
58. LIGG; Water and Energy Commission Secretariat (WECS); Nepal Electricity Authority (NEA). *Report on the First Expedition to Glaciers and Glacier Lakes in the Pumqu (Arun) and Poiqu (Bhote-Sun Koshi) River Basins, Xizang (Tibet), China*; Science Press: Beijing, China, 1988.
59. Su, Z.; Ding, L.; Liu, C.C. Glacier thickness and its reserves calculation on Tianshan Mountains. *Xinjiang Geogr.* **1984**, *7*, 37–44.

60. Haeberli, W.; Hoelzle, M. Application of Inventory Data for Estimating Characteristics of and Regional Climate-Change Effects on Mountain Glaciers: A Pilot Study with the European Alps. *Ann. Glaciol.* **1995**, *21*, 834. [[CrossRef](#)]
61. Ostrem, G. *Sediment Transport in Glacial Meltwater Streams*; Jopling, A.V., McDonald, B.C., Eds.; Glaciofluvial and Glaciolacustrine Sedimentation; Society of Economic Paleontologists and Mineralogists Special Publication SEPM Society for Sedimentary Geology: Broken Arrow, OK, USA, 1975; Volume 23, pp. 101–122.
62. Braithwaite, R.J. Can the mass balance of a glacier be estimated from its equilibrium-line altitude? *J. Glaciol.* **1984**, *30*, 364–368. [[CrossRef](#)]
63. Kulkarni, A.V. Mass balance of Himalayan glaciers using AAR and ELA methods. *J. Glaciol.* **1992**, *38*, 101–104. [[CrossRef](#)]
64. Pelto, M.S. Forecasting temperate alpine glacier survival from accumulation zone observations. *Cryosphere* **2010**, *4*, 67–75. [[CrossRef](#)]
65. Brahmabhatt, R.M.; Bahuguna, I.; Rathore, B.P. Variation of Snowline and Mass Balance of Glaciers of Warwan and Bhut Basins of Western Himalaya Using Remote Sensing Technique. *J. Indian Soc. Remote Sens.* **2012**, *40*, 629–637. [[CrossRef](#)]
66. Pelto, M.; Brown, C. Mass balance loss of Mount Baker, Washington glaciers 1990–2010. *Hydrol. Process.* **2012**, *26*, 2601–2607. [[CrossRef](#)]
67. Kulkarni, A.V.; Rathore, B.P.; Suja, A. Monitoring of glacial mass balance in the Baspa basin using accumulation area ratio method. *Curr. Sci.* **2004**, *86*, 101–106.
68. Dyurgerov, M.; Meier, M.F.; Bahr, D.B. A new index of glacier area change: A tool for glacier monitoring. *J. Glaciol.* **2009**, *55*, 710–716. [[CrossRef](#)]
69. Garg, S.; Shukla, A.; Garg, P.K.; Yousuf, B.; Shukla, U.K. Surface evolution and dynamics of the Kangriz glacier, western Himalaya in past 50 years. *Cold Reg. Sci. Technol.* **2022**, *196*, 103496. [[CrossRef](#)]
70. Oerlemans, J.; Hoogendoorn, N.C. Mass-balance gradients and climatic change. *J. Glaciol.* **1989**, *35*, 399–405. [[CrossRef](#)]
71. Haeberli, W. Glacier and permafrost signals of 20th-century warming. *Ann. Glaciol.* **1990**, *14*, 99–101. [[CrossRef](#)]
72. Kraaijenbrink, P.; Meijer, S.W.; Shea, J.M.; Pellicciotti, F.; Jong, S.D.; Immerzeel, W.W. Seasonal surface velocities of a Himalayan Glacier derived by automated correlation of unmanned aerial vehicle imagery. *Ann. Glaciol.* **2016**, *57*, 103–113. [[CrossRef](#)]
73. Harrison, W.D.; Elsberg, D.H.; Echelmeyer, K.A.; Krimmel, R.M. On the characterization of glacier response by a single timescale. *J. Glaciol.* **2001**, *47*, 659–664. [[CrossRef](#)]
74. Jóhannesson, T.; Raymond, C.; Waddington, E. Timescale for adjustment of glaciers to changes in mass balance. *J. Glaciol.* **1989**, *35*, 355–369. [[CrossRef](#)]
75. Bolch, T.; Kulkarni, A.; Kääb, A.; Huggel, C.; Paul, F.; Cogley, J.G.; Frey, H.; Kargel, J.S.; Fujita, K.; Scheel, M.; et al. The State and Fate of Himalayan Glaciers Science. *Science* **2012**, *336*, 310–314. [[CrossRef](#)]
76. Kulkarni, A.V.; Bahuguna, I.M.; Rathore, B.P.; Singh, S.K.; Randhawa, S.S.; Sood, R.K.; Dhar, S. Glacial retreat in Himalaya using remote sensing satellite data. *Curr. Sci. India* **2007**, *92*, 69–74. [[CrossRef](#)]
77. Mehta, M.; Dobhal, D.P.; Bisht, M.P.S. Change of Tipra Glacier in the Garhwal Himalaya, India, between 1962 and 2008. *Prog. Phys. Geogr.* **2011**, *35*, 721–738. [[CrossRef](#)]
78. Tawde, S.A.; Kulkarni, A.V.; Bala, G. Estimation of glacier mass balance on a basin-scale: An approach based on satellite-derived snowlines and a temperature index model. *Curr. Sci.* **2016**, *111*, 1977–1989. [[CrossRef](#)]
79. Majeed, U.; Rashid, I.; Najar, N.A.; Gul, N. Spatiotemporal dynamics and geodetic mass changes of glaciers with varying debris cover in the pangong region of Trans-Himalayan Ladakh, India between 1990 and 2019. *Front. Earth Sci.* **2021**, *9*, 748107. [[CrossRef](#)]
80. Kumar, V.; Mehta, M.; Shukla, T. Spatially resolved estimates of glacial retreat and lake changes from Gepang Gath Glacier, Chandra Basin, Western Himalaya, India. *J. Geol. Soc. India* **2021**, *97*, 520–526. [[CrossRef](#)]
81. Shukla, A.; Qadir, J. Differential response of glaciers with varying debris cover extent: Evidence from changing glacier parameters. *Int. J. Remote Sens.* **2016**, *37*, 2453–2479. [[CrossRef](#)]
82. Rashid, I.; Majeed, U. Recent recession and potential future lake formation on Drang Drung glacier, Zaskar Himalaya, as assessed with earth observation data and glacier modelling. *Environ. Earth Sci.* **2018**, *77*, 1–13. [[CrossRef](#)]
83. Azam, M.F.; Ramanathan, A.L.; Wagnon, P.; Vincent, C.; Linda, A.; Berthier, E.; Pottakkal, J.G. Meteorological conditions, seasonal and annual mass balances of Chhota Shigri Glacier, western Himalaya, India. *Ann. Glaciol.* **2016**, *57*, 328–338. [[CrossRef](#)]
84. Sherpa, S.F.; Wagnon, P.; Brun, F.; Berthier, E.; Vincent, C.; Lejeune, Y.; Arnaud, Y.; Kayastha, R.B.; Sinisalo, A. Contrasted surface mass balances of debris-free glaciers observed between the southern and the inner parts of the Everest region (2007–2015). *J. Glaciol.* **2017**, *63*, 637–651. [[CrossRef](#)]
85. Gardelle, J.; Berthier, E.; Arnaud, Y. Impact of resolution and radar penetration on glacier elevation changes computed from DEM differencing. *J. Glaciol.* **2012**, *58*, 419–422. [[CrossRef](#)]
86. Kääb, A.; Berthier, E.; Nuth, C.; Gardelle, J.; Arnaud, Y. Contrasting patterns of early twenty-first-century glacier mass change in the Himalayas. *Nature* **2012**, *488*, 495–498. [[CrossRef](#)]
87. Garg, S.; Shukla, A.; Garg, P.K.; Yousuf, B.; Shukla, U.K.; Lotus, S. Revisiting the 24 year (1994–2018) record of glacier mass budget in the Suru sub-basin, western Himalaya: Overall response and controlling factors. *Sci. Total Environ.* **2021**, *800*, 149533. [[CrossRef](#)]
88. Kulkarni, A.V.; Rathore, B.P.; Mahajan, S.; Mathur, P. Alarming retreat of Parbati Glacier, Beas basin, Himachal Pradesh. *Curr. Sci.* **2005**, *88*, 1844–1850.

89. Wagnon, P.; Linda, A.; Arnaud, Y.; Kumar, R.; Sharma, P. Four years of mass balance on Chhota Shigri Glacier, Himachal Pradesh, India, a new benchmark glacier in the western Himalaya. *J. Glaciol.* **2007**, *53*, 603–611. [[CrossRef](#)]
90. Berthier, E.; Arnaud, Y.; Kumar, R.; Ahmad, S.; Wagnon, P.; Chevallier, P. Remote sensing estimates of glacier mass balances in the Himachal Pradesh (Western Himalaya, India). *Remote Sens. Environ.* **2007**, *108*, 327–338. [[CrossRef](#)]
91. Dobhal, D.P.; Gergan, J.T.; Thayyen, R.J. Mass balance studies of the Dokriani Glacier from 1992 to 2000, Garhwal Himalaya, India. *Bull. Glaciol. Res.* **2008**, *25*, 9–17.
92. Raina, V.K.; Kaul, M.K.; Singh, S. Mass—Balance studies of Gara glacier. *J. Glaciol.* **1977**, *18*, 415–423. [[CrossRef](#)]
93. Srivastava, D.; Sangewar, C.V.; Kaul, M.K.; Jamwal, K.S. Mass balance of Rulung glacier—A Trans-Himalayan glacier, Indus basin, Ladakh. *Geol. Surv. India Spec. Publ.* **2001**, *53*, 41–46.
94. Sangewar, C.V.; Siddique, N.S. Thematic compilation of mass balance data on glaciers in Satluj catchment in Himachal Himalaya. *Geol. Surv. India Rep.* **2006**, *141*, 159–161.
95. Dobhal, D.P.; Kumar, S.; Mundepi, A.K. Morphology and glacier dynamics studies in monsoon–arid transition zone: An example from Chhota Shigri glacier, Himachal Himalaya, India. *Curr. Sci.* **1995**, *68*, 936–944.
96. Azam, M.F.; Wagnon, P.; Ramanathan, A.; Vincent, C.; Sharma, P.; Arnaud, Y.; Linda, A.; Pottakkal, J.G.; Chevallier, P.; Singh, V.B.; et al. From balance to imbalance: A shift 15 in the dynamic behavior of Chhota Shigri Glacier (Western Himalaya, India). *J. Glaciol.* **2012**, *58*, 315–324. [[CrossRef](#)]
97. Swaroop, S.; Gautam, C.K. Glaciological studies on Dunagiri Glacier, Chamoli district, Uttar Pradesh. *Geol. Surv. India Rec.* **1990**, *24*, 186–190.
98. Srivastava, D.; Swaroop, S.; Mukerji, S.; Gautam, C.K.; Roy, D. Suspended sediment yield and its variation in Dunagiri Glacier melt stream, Garhwal Himalaya. In Proceedings of the Symposium on Snow, Ice, and Glaciers—A Himalayan Perspective, Lucknow, India, 9–11 March 1999; p. 45.
99. Koul, M.N.; Ganjoo, R.K. Impact of inter and intra-annual variation in weather parameters on mass balance and equilibrium line altitude of Naradu Glacier (Himachal Pradesh), NW Himalaya, India. *Clim. Chang.* **2010**, *99*, 119–139. [[CrossRef](#)]
100. Aizen, V.B.; Aizen, E.M.; Nikitin, S.A. Glacier regime on the northern slope of the Himalaya (Xixibangma glaciers). *Quat. Int.* **2002**, *97*, 27–39. [[CrossRef](#)]
101. Ostrem, G. Ice melting under a Thin Layer of Moraine, and the existence of ice cores in Moraine Ridges. *Geogr. Ann.* **1959**, *41*, 228–230. [[CrossRef](#)]
102. Li, J.; Su, Z. *Glacier in Hengduan*; Mountains Science Press: Beijing, China, 1996.
103. Nicholson, L.; Benn, D.I. Calculating ice melt beneath a debris layer using meteorological data. *J. Glaciol.* **2006**, *52*, 463–470. [[CrossRef](#)]
104. Quincey, D.J.; Copland, L.; Mayer, C.; Bishop, M.; Luckman, A.; Belò, M. Ice velocity and climate variations for Baltoro Glacier, Pakistan. *J. Glaciol.* **2009**, *55*, 1061–1071. [[CrossRef](#)]
105. Brun, F.; Wagnon, P.; Berthier, E.; Shea, J.M.; Immerzeel, W.W.; Kraaijenbrink, P.D.; Arnaud, Y. Ice cliff contribution to the tongue-wide ablation of Changri Nup Glacier, Nepal, central Himalaya. *Cryosphere* **2018**, *12*, 3439–3457. [[CrossRef](#)]

**Disclaimer/Publisher’s Note:** The statements, opinions and data contained in all publications are solely those of the individual author(s) and contributor(s) and not of MDPI and/or the editor(s). MDPI and/or the editor(s) disclaim responsibility for any injury to people or property resulting from any ideas, methods, instructions or products referred to in the content.